Comparison of three different Modulators for Power Converters with Respect to EMI Optimization

Knott, Arnold; Pfaffinger, Gerhard; Andersen, Michael Andreas E.

Published in:
2008 IEEE International Symposium on Industrial Electronics

Link to article, DOI:
10.1109/ISIE.2008.4676962

Publication date:
2008

Document Version
Publisher's PDF, also known as Version of record

Comparison of three different Modulators for Power Converters with Respect to EMI Optimization

Arnold Knott * †, Gerhard Pfaffinger †, Michael A.E. Andersen *
* Technical University of Denmark
Elektrovej, bygning 325
2800 Kgs. Lyngby, Denmark
† Harman/Becker Automotive Systems GmbH
Schlesische Str. 135
94315 Straubing, Germany

***Abstract*—Switch-mode Power Converters are well known for emissions in the band of electromagnetic interference (EMI) interest. The spectrum shape depends on the type of modulator and its purpose. This paper gives design guidelines to choose the optimum topology depending on requirements of different applications. Spectral measurements on prototypes of a pulse width modulator (PWM), a $\Delta\Sigma$-modulator and a hysteretic self-oscillating modulator are shown, which are verifying their simulations, with respect to different EMI challenges.**

I. Introduction

Modulators for power converters transfer a reference signal into a switching signal with a discrete number of levels, which is in many cases high and low only. By doing this conversion, the modulator is adding much energy above the frequency of the reference signal. This energy is distributed over a wide range of frequencies, which are measured in EMI tests. The standards for EMI (i.e. [1]) give especially low limits in the sensitivity bands of receivers of broadcasting technologies, such as AM radio, terrestrial TV and FM radio. Due to the high required dynamical range and - depending on the location - weak signal strengths, these limits are very low.

One of the most interesting scenarios are therefore applications, where the switch-mode power converter is very close to the receiver and the coupling path from the converter – as an EMI source – to the receiver – as an EMI sink – is very low ohmic. Both of those conditions are fulfilled in cars: the separation of the source and the sink is only a few meters, resulting in enhanced radiated coupling. Common supply lines, electrical communication lines as well as the chassis give good conduction conditions. Additionally it is a primary design goal for the receivers to reach very low sensitivity levels, because the antenna can not be set up in an optimized way and kept there as in consumer applications due to the movement of the vehicle.

There are two different worst case situations for tuners: one is the seek mode and the other one is a low input signal. In the seek mode, tuners are sweeping the sensitivity window as fast as possible through their input band and try to detect a carrier of a broadcasting station. If there is any single frequency component emitted from a power converter, the tuner is likely to lock into this frequency but unfortunately the side bands are not the program material from a radio or TV station, but the sidebands of the distortion signal. In the second case, the tuner has already locked to a station, but has only weak signal. If the broadband noise from a power converter is overdriving the sidebands of this carrier, the broadcasted program material is again lost and the noise of the converter in this band is displayed on the screen or played through the audio system. Actual receiver input characteristics, frequency bands and their related noise levels have been described in [2] and [3]

An interesting application, which by itself have an EMI source as well as an EMI sink, as described above, close to each other are automotive audio amplifiers. Many of those either comprehend a switch-mode power supply or the amplifier itself is a Class-D type or both of those are combined. In case of audio amplifiers another frequency band is of high interest: the audio band from 20 Hz to 20 kHz. The performance measurements in this band are given by [4], where the according measurements results are highly competitive.

Other applications in many consumer, industrial or automotive products like DC/DC-converters, motor drives or switch-mode power amplifiers deal with the same EMI sinks. The comparison shown in this paper is applicable to those without change. Figure 1 shows a typical block diagram of a Class-D amplifier, including an error amplifier, a modulator, level shifter and gate driver, a power stage and a fourth order output filter.

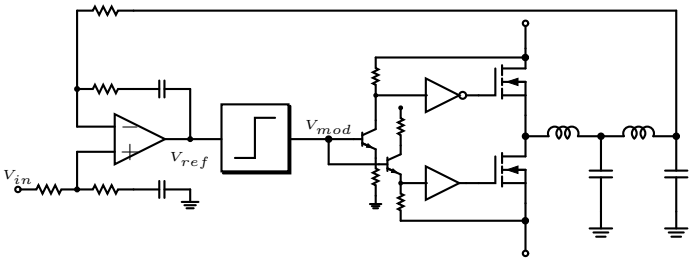

Fig. 1. Block diagram of a typical realization of a switch-mode power amplifier

In many realizations a fourth order output filter and shielding is required to fulfill the EMI requirements. The fourth

978-1-4244-1666-0/08/$25.00 ©2008 IEEE

order filter significantly decreases the performance in the audio band, adds cost, board space and weight to the application. The shields to return the stray fields of the modulator, power stage and inductors usually cause a trade-off between thermal optimized mechanical design and EMI. Some of the electro-magnetic fields can be annihilated by parasitic cancellation in the filter components. These techniques have been described in [5], [6], [7] and [8].
A practical approach to change the high frequency energy distribution is called randomized PWM and EMI investigations on DC-DC converters for automotive use are shown in [9]. These technologies are not considered here because they are known to introduce the randomized noise also in the audio band and therefore significantly decrease the performance.
A typical EMI measurement result on a converter according to the block diagram in figure 1 and optimized component selection and layout is shown in figure 2. The measurement is the worst case measurement within a series of differential and common mode EMI measurements in various distances between the current probe and the output of the converter. The measurements where done in accordance to the current method in [1] as well as to the specification of one car manufacturer. The car manufacturers limits are more stringent in the receiver bands and mandatory to fulfill in the original equipment manufacturer market (OEM). Similar measurements aligned with the voltage method described in CISPR25 [1] are shown in [10].

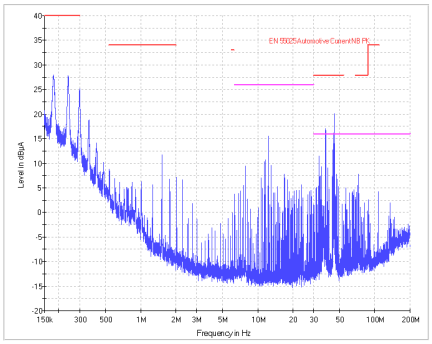

Fig. 2. Common Mode EMI measurement (current probe method) on the output lines of an automotive audio power amplifier

While many design approaches concentrate on the removal of the EMI noise, this paper will concentrate on the modulators, which are adding the high frequency energy to the system. It first explains the three different modulator topologies in section II. Simulation results with respect to the out-of-band behavior based on functional description models of these modulators are shown in section III. As an experiment prototypes of the modulators have been built and the spectra where measured which are shown in section IV. Section V compares the spectra of the modulators and different modulation indices in perspective to the relevant criteria for optimized broadcasting service reception and section VI concludes the behavior of an optimized modulator for all relevant tuner scenarios.

II. Modulator Topologies

Following is a description of the functionality of a PWM, a $\Delta\Sigma$ modulator and a hysteretic self-oscillating modulator. Common requirement to all modulators is the capability of accepting an audio frequency input signal and modulate it into a discrete level output signal while maintaining the input signal. The modulators must not add energy within the audio frequency range and the switching frequencies at the output are supposed to be configurable to a range between 200 kHz and 800 kHz. This is assumed to be a frequency range where the power stages consisting of MOSFETs and the output filters can operate in an efficiency optimized region.

A. Pulse Width Modulator

Figure 3 shows the block diagram of a PWM. It consists of an oscillator, an integrator and a comparator. The oscillator needs to generate a square wave clock, which is integrated to a triangle or a sawtooth. This signal is compared to a reference signal which is the output of the differential error amplifier in figure 1. Depending on which of these two signals is higher, the output of the comparator is either high or low.

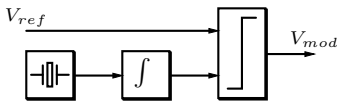

Fig. 3. Block diagram of a PWM

The reference signal determines between natural PWM (continuous time input signal) and uniform PWM (discrete time input signal). Two levels at the output are described in the literature [11] as AD modulation, while three output level signals are described as BD modulation. A triangle as carrier input to the comparator results in a double side PWM, while a sawtooth creates a single side PWM. For simulation and experiment a natural sampled AD two side modulated PWM (NADD PWM) is used.
The decomposition of an NADD PWM output signal into its spectral components by a double Fourier series (DFS) as described in [12] gives an expectation of the PWM spectrum as shown in equation 1

$$PWM(t) = k + \frac{M}{2}\cos(\omega_{ref}t) + \sum_{m=1}^{\infty}\frac{\sin(m\omega_{clk}t)}{m\pi} - \sum_{m=1}^{\infty}\frac{J_0(m\pi M)}{m\pi}\sin(m\omega_{clk}t - 2m\pi k) - \sum_{m=1}^{\infty}\sum_{n=\pm1}^{\pm\infty}\sin(m\omega_{clk}t + n\omega_{ref}t - 2m\pi k - \frac{n\pi}{2}) \quad (1)$$

where k is the offset of the signal, M is the modulation index, ω_{ref} the radian frequency of the sinusoidal reference signal,

J_n the n-th order Bessel function of the first kind and ω_{clk} the radian frequency of the carrier signal and m and n are integer numbers.

B. Delta-Sigma Modulator

The $\Delta\Sigma$ modulator block diagram is shown in figure 4. The Δ-stage subtracts the output from the reference, which is again the output of the differential error amplifier as shown in figure 1, the Σ-stage is an integrator summing up the difference signal and feeding a comparator. This comparator is changing its output in dependency of the integrator signal being higher or lower as a constant reference. A latch, i.e. a D-type flip-flop, is transferring the comparator output pulses triggered by a rectangular clock signal derived from an oscillator. The oscillator frequency with a $50\ \%$ duty cycle is adjusting the main switching frequency. The main switching frequency is expected to be half of the clock frequency, when using a positive edge triggered flip-flop.

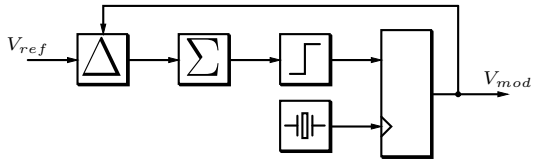

Fig. 4. Block diagram of a $\Delta\Sigma$ modulator

C. Hysteretic Self-Oscillating Modulator

The hysteretic self-oscillating modulator is described in [13]. Compared to the PWM and $\Delta\Sigma$ it does not require an external clock but deriving its switching frequency by operating at the stability boundary. The reference signal from the error amplifier is summed and integrated together with the output signal and fed into a hysteretic comparator. A block diagram is shown in figure 5.

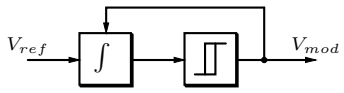

Fig. 5. Block diagram of an hysteretic self-oscillating modulator

The switching frequency of a hysteretic self-oscillating modulator is determined by M, the time constant of the integrator τ_{int}, the hysteretic window H and the propagation delay of the forward path τ_{pd} as shown in equation 2.

$$\omega_{sw} = \frac{1 - M^2}{8\pi(\tau_{int}H + \tau_{pd})} \tag{2}$$

III. Simulation

The simulation of the described modulators was carried out in the time domain with linearized blocks, followed by a Fourier transformation calculated by MATLAB. The switch-mode elements where modeled as discrete two level outputs and no edges where taken into account. Within the considered frequency range, this is a valid assumption. For optimal comparison of the three modulators, the clock frequency was set to the same frequency $f_{clk} = 270$ kHz. The supply voltage was 5 V for ideal comparison with the measurements in the experiment shown in section IV.

Figure 6(a) shows the simulated spectrum of an NADD PWM with the modulation indices $M = 0$, $M = 0.3$ and $M = 1$. As expected from equation 1 side bands with distance f_{ref} are growing around the switching frequency f_{clk} with increasing modulation. The spectral components are situated at discrete frequencies, which reflects the repetitive nature of a PWM bit stream in time domain. The noise level of the simulation is limited to the timing precision of the simulation which was chosen to a compromise between simulation time and resolution in the results.

The comparable results for a $\Delta\Sigma$ modulator are shown in figure 6(b). The decision points of a $\Delta\Sigma$ modulator are based on the input signal as well as on the noise fed back from the output. This noise is modeled as white noise [14]. This noise is uncorrelated and therefore the bit stream pattern of a $\Delta\Sigma$ modulator is non repetitive in time domain which results in a continuous spectrum shape. As the basic shape in time domain at $M = 0$ is close to a rectangular waveform with $50\ \%$ duty cycle and the height of these pulses is - as in the PWM - limited by the supply voltage of the output stage. Therefore the peaks stay at the same level, and the side bands are filled with energy, while the inherent noise shaping nature of the modulator removes noise between the harmonics. At higher modulation indices the minima in the spectrum remain but the side bands are continuously filled with energy. The overall energy in the out-of-band noise of a $\Delta\Sigma$ modulator is therefore higher than the noise of a PWM.

The simulation results of a hysteretic self oscillating modulator is shown in figure 6(c). In case of $M = 0$, no source is applied to the modulator and no quantization noise is added. The peaks in the spectrum are equivalent to a stable rectangular signal with $50\ \%$ duty cycle - as in the PWM case - while the spectral resolution is limited to the Fourier transformation. With increasing modulation index sidebands around the carrier occur and the inherent feedback shows a portion of the same noise shaping effect as seen by the $\Delta\Sigma$ modulator. A full level input signal shifts the switching frequency towards the input frequency and creates harmonics based on the new fundamental.

IV. Experiment

This section will take the simulation in perspective to measurements on prototypes of the modulators as shown in figure 7. All measurements where taken with a Rohde & Schwarz ESI17 EMI test receiver in spectrum analyzer mode. The measurement bandwidth was 500 Hz, number of taken points was 500. The clocks and the reference signals were fed into the modulators from function generators. The outputs of the modulators where actively divided by 40 dB because the modulator outputs where not designed to drive the $50\ \Omega$ inputs of the analyzer. For best comparison with simulation the results were plotted, after recovering the 40 dB correction factor, with MATLAB. During the measurements

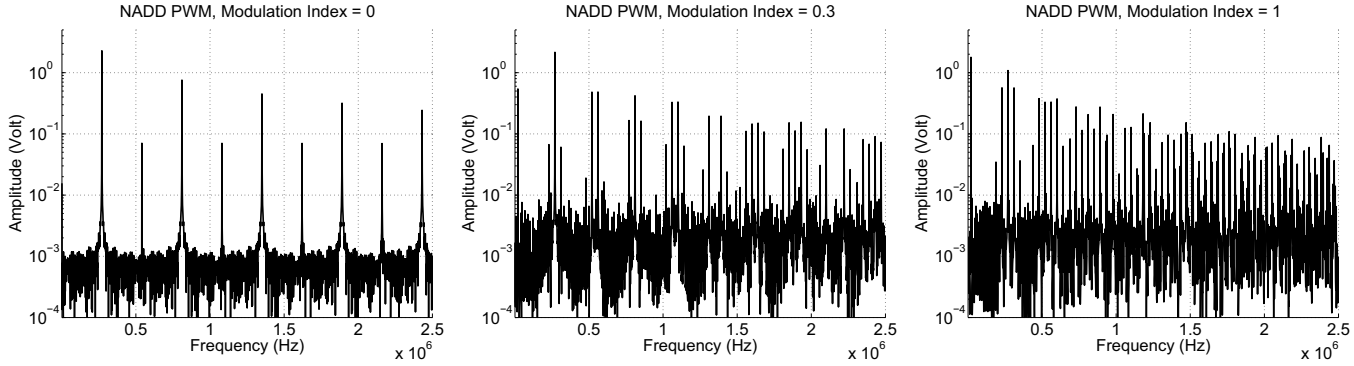

(a) NADD PWM

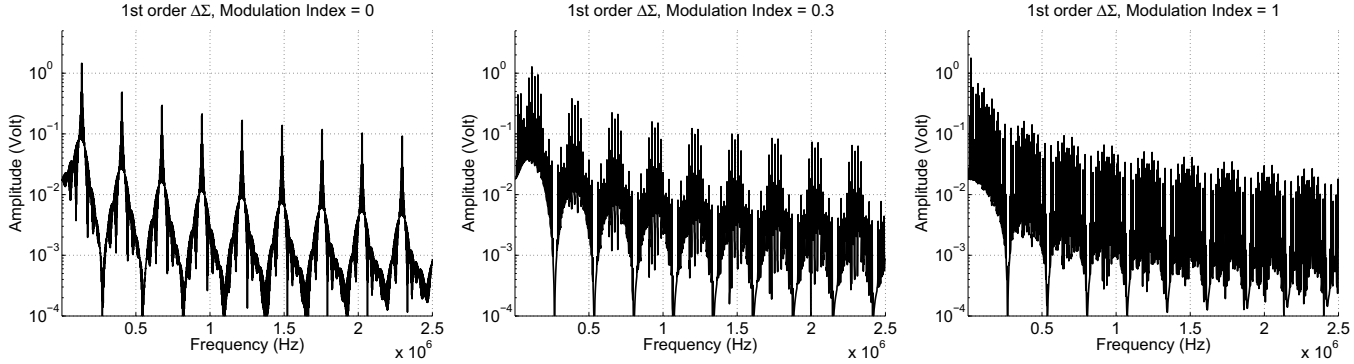

(b) $\Delta\Sigma$ modulator

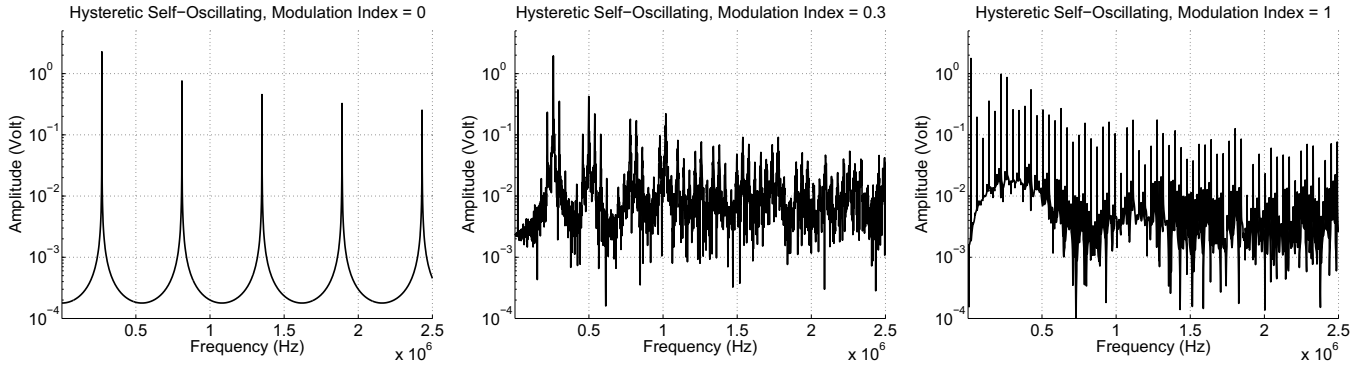

(c) Hysteretic Self-Oscillating

Fig. 6. Simulated spectra

the rectangular signals as well as all inputs were supervised in time domain with an oscilloscope.

Figure 8(a) shows the measurement results on the PWM. As predicted by simulation, the spectrum contains discrete components only. The even harmonics at $M = 0$ are an artifact of the imperfect symmetry of the triangular carrier. The measurements show the discrete side bands rising with increased modulation. The peak height is well aligned with the simulation results.

The same measurements have been carried out on the $\Delta\Sigma$ modulator prototype. Results are shown in figure 8(b). For $M = 0$ the spectral minima are masked by the noise level of the spectrum analyzer. This is a result of an trade-off between measurement time and accuracy. For longer measurement times and smaller measurement bandwidth the noise level of the analyzer can be significantly decreased. For higher modulation the noise level of the modulator is raised as predicted by simulation and the dips of the modulator dominate the noise level of the measurement system. The non-repetitive nature of a $\Delta\Sigma$ bit stream in time domain clearly results in a continuous spectrum. A full level modulation shows a dramatic increase in overall high frequency energy. The local minima in the spectrum stay consistent and have the width of twice the reference signals frequency f_{ref}. The increased noise reaches the audio band. An additional noise shaping is required to preserve the in-band performance. The $\Delta\Sigma$ modulator is likely

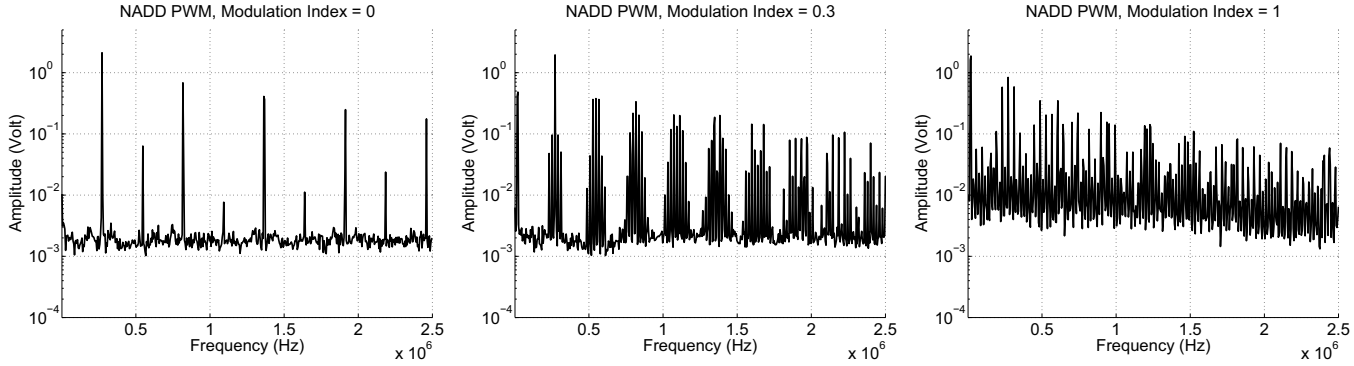

(a) NADD PWM

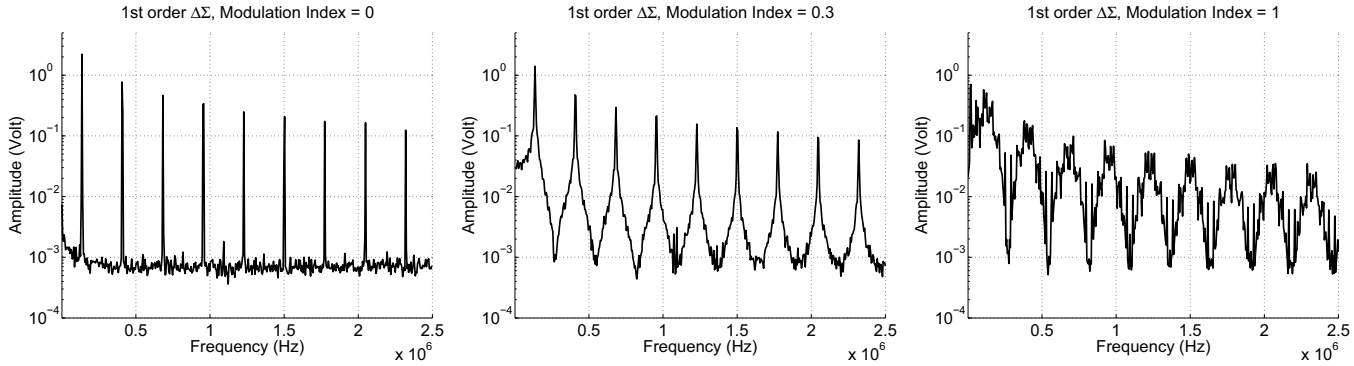

(b) $\Delta\Sigma$ modulator

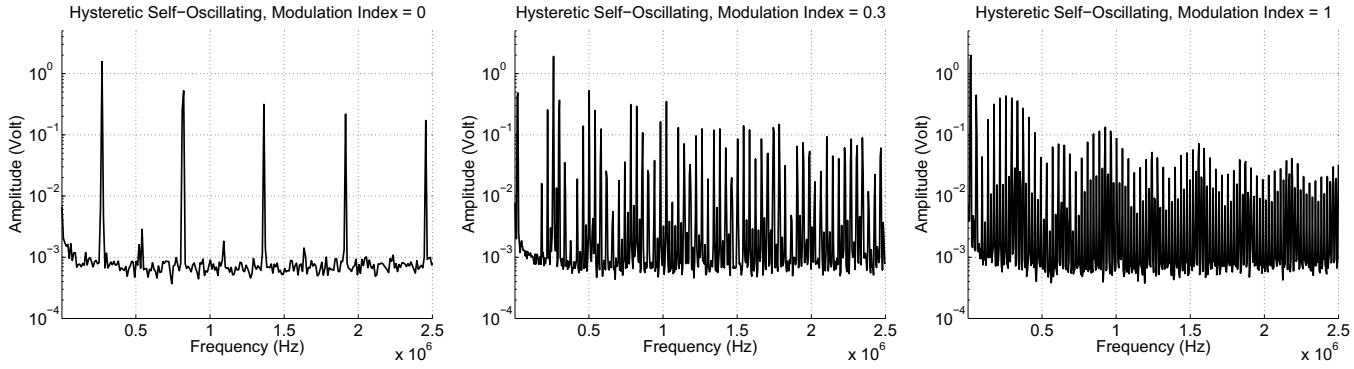

(c) Hysteretic Self Oscillating

Fig. 8. Measured spectra

to run into stability problems at high modulation indices as researched in [15] and more recently in [16]. Practically the modulation indices in these systems therefore are limited.

The hysteretic self-oscillating modulator was tested in the same measurement setup as the above shown and results are shown in figure 8(c). Without any input signal the hysteretic self-oscillating modulator produces very perfect rectangular waveform with 50 % duty cycle, independent of any external signal sources. Therefore the even harmonics of the switching frequency at zero modulation $f_{ref}|_{M=0}$ are close to zero. Remaining imperfections only belong to the nonlinearity of the modulator components. With increasing modulation the switching frequency drops (in figure 8(c) from 273 kHz to 248 kHz). More discrete side bands occur than in the PWM case. For full modulation the decision points are forced by the input signal and the fundamental of the switching frequency $f_{sw}|_{M=1}$ drops to the input frequency $f_{ref} = 20$ kHz. Equation 2 does not take the forced commutation into account.

V. Comparison of Results

The shown simulated and measured spectra will be taken into perspective to receivers input sensitivity scenarios as explained in section I here. The main interesting parameters are the local maxima (peaks, table I), local minima (dips, table II) of the spectrum, the side bands around the carrier (table III) and the noise performance in the audio band (table IV). The height of the peaks is directly related to the probability of

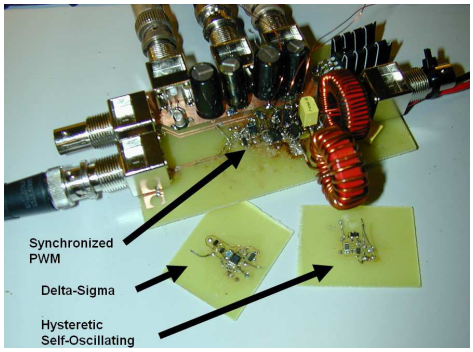

Fig. 7. Picture of Prototypes

a receiver locking accidentally into it and considering the peak as carrier of a broadcasting station. The dips allow receivers to detect very low signals because the minimum signal strength of the program material can be just slight above the dips. The side bands around the carrier act directly opposed to that and might overdrive program material of a station. The noise performance in the audio band does not disturb the receivers but is directly transferring audible noise through the power stage to the speaker. Again the program material, even if coming from a recorded source might be hidden below this noise level.
The rules for comparison and conclusions result in preferably

- low maxima (peaks),
- wide and low minima (dips),
- narrow, predictable and low side bands and
- low and frequency independent noise in the audio band.

PEAKS	PWM	ΔΣ	HSO
$M = 0$	$n \cdot f_{clk}$	$\frac{2 \cdot n}{2} f_{clk}$	$n \cdot f_{sw}\|_{M=0}$
$M = 0.3$	$n \cdot f_{clk}$ & $n \cdot f_{clk} \pm m \cdot f_{ref}$	$\frac{2 \cdot n}{2} f_{clk}$ & $\frac{2 \cdot n}{2} f_{clk} \pm m \cdot f_{ref}$	$n \cdot f_{sw}\|_{M=0}$ & $n \cdot f_{sw}\|_{M=0} \pm m \cdot f_{ref}$
$M = 1$	$n \cdot f_{clk}$ & $n \cdot f_{clk} \pm m \cdot f_{ref}$	spread at $\frac{2 \cdot n}{2} f_{clk} \pm m \cdot f_{ref}$	$m \cdot f_{ref}$

TABLE I
COMPARISON OF LOCAL MAXIMA IN THE DIFFERENT MODULATORS

Common to all three modulators is that the peaks are decreasing with increasing modulation index.

DIPS	PWM	ΔΣ	HSO
$M = 0$	practically limited to the noise floor by the dynamical range of the sytem	$n \cdot f_{clk}$	practically limited to the noise floor by the dynamical range of the system
$M = 0.3$		$n \cdot f_{clk}$	
$M = 1$		$n \cdot f_{clk} \pm f_{ref}$	

TABLE II
COMPARISON OF LOCAL MINIMA IN THE DIFFERENT MODULATORS

While the noise floor in PWM and hysteretic self-oscillating are system limitations, is the spectrum of a ΔΣ an intrinsically shaped form.

SIDE BANDS	PWM	ΔΣ	HSO
$M = 0$	equivalent to the frequency stability of the oscillator	continuous	frequency stability equivalent to an RC-oscillator
$M = 0.3$	discrete, frequency stability dependent on input and on stability of the oscillator		discrete, frequency stability equivalent to an RC-oscillator and dependent on input signal
$M = 1$	discrete, many frequencies due to intermodulation		

TABLE III
COMPARISON OF SIDE BANDS AROUND THE CARRIER AND ITS HARMONICS

ADUIO NOISE	PWM	ΔΣ	HSO
$M = 0$	constant	noise shappped	constant
$M = 0.3$			
$M = 1$	side bands may occur in audio band		

TABLE IV
COMPARISON OF AUDIO BAND NOISE

The best behavior for each modulation level is shaded gray in the tables based on the explained comparison rules.
Some related modulator technologies can extend this list, i.e. NBDD modulated PWM, which is removing differential peaks compared to what is shown in the NADD example, a

$\Delta\Sigma$ modulator of second order including intrinsically noise shaping or noise shaped $\Delta\Sigma$ modulators as well as phase shifted self oscillating systems. Two interesting approaches to influence the spectral behavior based on PWM are shown in [17] called predistorted PWM (Pd-PWM) and frequency modulated PWM (FM-PWM).

VI. Conclusion

The relevance of the EMI behavior of modulators has been explained with respect to potential EMI sinks, especially TV and radio receivers. Therefore four relevant parameters (maxima, minima, side bands and base band noise) to weight the performance have been defined. Three different types of modulators (PWM, $\Delta\Sigma$ and hysteretic self-oscillating) have been explained, simulated and verified by measurements on prototypes. The measurements match the simulations. The results have been summarized with respect to the criteria relevant for receivers. The characteristics of an optimal modulator as combination of all advantages has been found.

The PWM and the hysteretic self-oscillating modulator show very similar spectral behavior. In applications where the peak detection of a nearby receiver is the most critical situation, the hysteretic self-oscillating modulator shows slight advantages. If detection of very low signal strength of the broadcasting system is the design priority, PWM is the best modulation topology. $\Delta\Sigma$ offers spectral dips which can be used to detect low signals when a tuner is already locked into the carrier of a broadcasting station. This advantage of a $\Delta\Sigma$ shows best up at high modulation indices where the modulator tends to be instable.

Additionally an outlook to other topologies was given. Depending on the strived design, a modulator can be chosen based on the given parameterization for many applications such as switch-mode power amplifiers and supplies or motor drives.

Acknowledgment

This research work was carried out with the kind support of Harman/Becker Automotive Systems GmbH.

References

[1] International Special Committee on Radio Interference. Electromagnetic disturbances related to electric / electronic equipment on vehicles and internal combustion engine powered devices. Standard CISPR/D/247/CD, International Electrotechnical Commission (IEC), Februar 2001.

[2] Jerry C. Whitaker. *The Communications Facility Design Handbook*. CRC Press, Boca Raton, 2000.

[3] Dorf, R.C.; Wan, Z.; Lindsey III, J.F.; Doelitzsch, D.F.; Whitaker J.; Roden, M.S.; Salek, S.; Clegg, A.H. *Broadcasting The Electrical Engineering Handbook*. CRC Press, Boca Raton, 2000.

[4] Audio Engineering Society Inc. AES standard method for digital audio engineering - Measurement of digital audio equipment. Standard AES17, AES Standards, March 1998.

[5] Liu, D.H.; Jiang, J.G. High frequency characteristic analysis of EMI filter in switch mode power supply (SMPS). *Power Electronics Specialists Conference*, Vol. 4, 2002.

[6] Wang, C.P.; Liu, D.H.; Jiang Jianguo. Study of coupling effects among passive components used in power electronic devices. *Power Electronics and Motion Control Conference*, Vol. 3, 2004.

[7] Liyu Yang; Bing Lu; Wei Dong; Zhiguo Lu; Ming Xu; Lee, F.C.; Odendaal, W.G. Modeling and characterization of a 1 KW CCM PFC converter for conducted EMI prediction. *Applied Power Electronics Conference and Exposition*, Vol. 2, 2004.

[8] Shuo Wang. *Characterization and Cancellation of High-Frequency Parasitics for EMI Filters and Noise Separators in Power Electronics Applications*. PhD thesis, Virginia Polytechnic Institute and State University, Blacksburg, Virgina, May 2005.

[9] Mihalic, F.; Kos, D. Conductive EMI reduction in DC-DC converters by using the randomized PWM. *Industrial Electronics, 2005. ISIE 2005. Proceedings of the IEEE International Symposium on*, Vol. 2:809–814, June 2005.

[10] Kos, D.; Mihalic, F.; Jezernik, K. Conductive EMI reduction in switched-mode power converters. *Industrial Electronics, 2005. ISIE 2005. Proceedings of the IEEE International Symposium on*, Vol. 2:441–446, June 2005.

[11] Pedersen, Michael Smedegaard; Shajaan, Mohammad. All Digital Power Amplifier Based on Pulse Width Modulation. *Audio Engineering Society Preprints*, 96th convention(3809), February 1994.

[12] Harold S. Black. *Modulation Theory*. van Nostrand Reinhard Company, 1953.

[13] Poulsen, S.; Andersen, M.A.E. Simple PWM modulator topology with excellent dynamic behavior. *Applied Power Electronics Conference and Exposition*, Vol. 1, 2004.

[14] Gray, Robert M. Spectral Analysis of Quantization Noise in a Single-Loop Sigma-Delta Modulator with dc Input. *IEEE Transactions on Communications*, Vol. 37(6):588–599, 1989.

[15] Risbo, L. $\Sigma - \Delta$ *Modulators — Stability Analysis and Optimization*. PhD thesis, Technical University of Denmark, Kgs. Lyngby, Denmark, June 1994.

[16] Antunes, V.M.E.; Pires, V.F.; Silva, J.F. Digital multilevel audio power amplifier with a MASH sigma-delta modulator to reduce harmonic distortion. *Industrial Electronics, 2005. ISIE 2005. Proceedings of the IEEE International Symposium on*, Vol. 2:525–528, June 2005.

[17] Xin Geng. *Design and Analysis of Pulse-Width Modulation Techniques for Spectrum Shaping*. PhD thesis, University of Illinois at Urbana-Champaign, Urbana-Champaign, Illinois, USA, 2007.